Chapter 2

System modelling

In order to apply state space adaptive control to a system, a comprehensive model has to be established for two reasons. Firstly, a precise model is needed for simulation purposes, and secondly a linear state space model can be derived from the previous one. The process of system modelling is topic of this chapter.

> "*A system is a potential source of data*", [Cellier, 1991].

A system is characterised by its bounds which define what belongs to it and what does not. Additionally, a system interacts with its environment through inputs which can influence the system behaviour, and its outputs which are determined by the system and can influence the environment. A system is the basic objective of scientific work. In the present case, the system under investigation is a rotor suspended in active magnetic bearings, and excited by non-conservative cross-coupling forces. This system does not exist *per se* but in specific implementations.

2.1 Experimental setup

Since no real application is accessible for testing new algorithms, an experimental setup is needed to make scientific investigations possible.

> "*An experiment is the process of extracting data from a system by exerting it through its inputs*", [Cellier, 1991].

To perform an experiment, it is necessary to set up a test rig. At the Institute for Machine Dynamics and Measurement, University of Technology Vienna, a test rig was built to test different algorithms for adaptive control in conjunction with non-conservative cross-coupling effects (see Fig. 2.1 and for a detailed description see [Lang, 1997]). Three actuators with backup bearings are mounted on a foundation. The outer actuators are used as active magnetic bearing, the central one as a magnetic exciter for the application of non-conservative cross-coupling forces to the rotor. In each actuator housing two proximity sensors are mounted operating as eddy current sensors. An

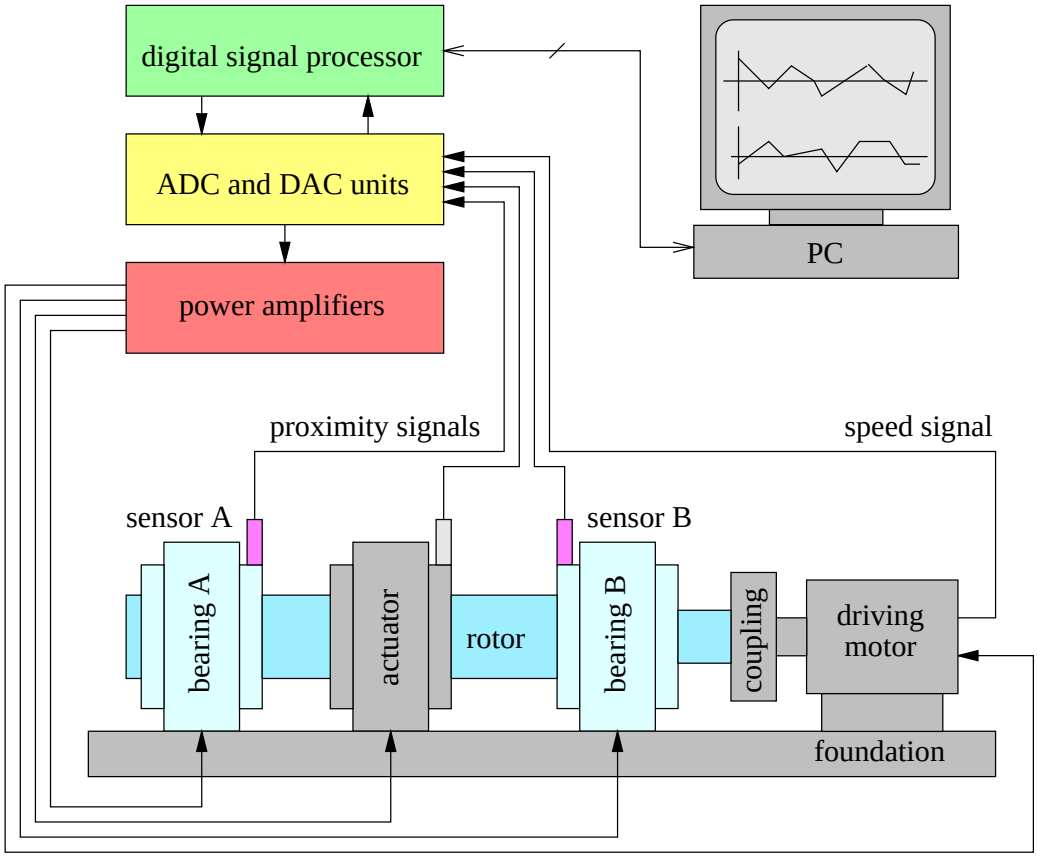

Figure 2.1: Experimental setup used for the real time implementation of adaptive control algorithms.

electric motor with a speed sensor is mounted on the foundation and drives the rigid rotor through an elastic coupling. The sensor signals are sampled by ADCs and fed into the digital signal processor (DSP) which performs the entire control task. The control variables are passed to the switching amplifiers via DACs. All actuators and the motor are driven by power amplifiers located in an electric console. The DSP-board is connected to a host computer for the sake of data acquisition and compilation of the digital signal processing code.

The presented test rig is to realise tests for adaptive control algorithms by means of the third actuator which can simulate any bearing behaviour. Before an algorithm is tested on that experimental setup, its performance must be tested and well proved by means of numerical simulation.

"*Simulation is an experiment performed on a model*", [Cellier, 1991].

The major motivation for simulation lies in the fact that more situations can be tested than in a real experimental setup without destroying anything. The facilities and the quality of the simulation runs depend on the model it is based upon. Therefore, a comprehensive mathematical model is required.

2.2 Comprehensive nonlinear model

Based upon the experimental setup, a model is derived for the sake of simplification and in order to make system analysis and simulation possible.

"*Modelling is mapping one system to another*", [Wurmsdobler, 1997].

Figure 2.2 shows a block diagram of the model for the given system as depicted in Fig. 2.1. The presented model is used for both simulation and derivation of a linear model. External inputs to the entire system shown in Fig. 2.2 are the set point, which is of course an internal input within the DSP and the measurement noise, output is the position of the rotor. The magnetic actuator applying the non-conservative

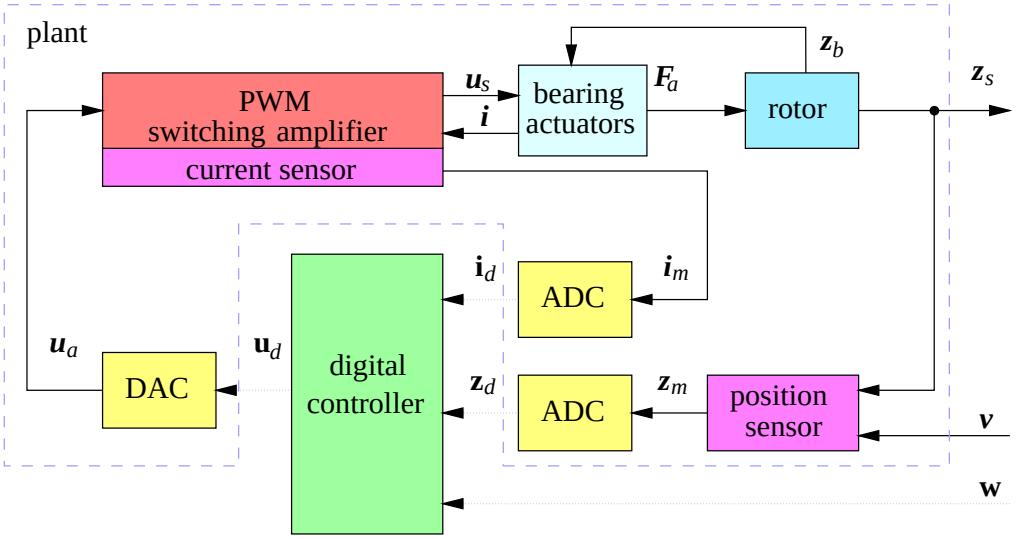

inputs: $\mathbf{w}$ set point
$\boldsymbol{v}$ measurement noise

output: $\mathbf{z}_s$ rotor position

internal variables:

$\mathbf{u}_d$	digital control voltage	$\boldsymbol{z}_b$	bearing coordinates
$\boldsymbol{u}_a$	analogue control voltage	$\boldsymbol{z}_s$	sensor coordinates
$\boldsymbol{u}_s$	switched voltage	$\boldsymbol{z}_m$	measured position
$\boldsymbol{F}_a$	actuator forces	$\boldsymbol{i}_m$	measured current
$\boldsymbol{i}$	current	$\mathbf{z}_d$	sampled position
		$\mathbf{i}_d$	sampled current

Figure 2.2: Block diagram of the entire system showing the inputs "measurement noise" and "set point", the output "rotor position" and all internal variables and subsystems.

cross-coupling forces to the rotor is not included and simulated in this work because

it is considered to be an independent control task and therefore, it is no objective for adaptive control. In a real experimental application the simulation of the cross-coupling forces has to be separated from the adaptive control law either by a separate hardware or logically, see [Lang, 1997].

The same is true for the speed control. The rotor is simply assumed to run at a certain speed. Additionally, no unbalance is introduced in the modelling process and simulated, because the resulting vibrations mask the adaptation effects. It would be difficult to distinguish between those vibrations and possible oscillations generated by the adaptive control algorithm. Of course, simulations can be carried out including unbalance, after the adaptation algorithm has been tested in order to gain a realistic simulation.

Once the bounds, the inputs and outputs of the system are defined the knowledge about the system has to be organised and mapped onto mathematical equations. Of course, this process has to be done hierarchically by defining the inputs and outputs of all subsystems (or modules) and their interactions. All subsystems are explained in detail within the following subsections. The corresponding MATLAB/SIMULINK block diagram models can be seen in Appendix D.1. The block diagram of the entire system is shown in Fig. D.1 and in detail in Fig. D.2.

2.2.1 Digital controller

The controller is implemented in a digital signal processor (Texas Instruments TMS320C40) and executes the control laws within the sampling period $T_s = 100\,\mu$s. Inputs are the measured and sampled currents of all magnets of both bearing actuators $\mathbf{i}_d$ and the measured and sampled rotor positions in the planes of the position sensors $\mathbf{z}_d$. Outputs are the digital control voltages for all magnets of both actuators $\mathbf{u}_d$. The corresponding block diagram can be seen in Fig. 2.3.

The operation of the DSP itself is not topic of this work. The algorithm for the computation of the control voltage $\mathbf{u}_d$ is explained in detail in Subsection 2.3.2 and Subsection 4.1.2 as for the current controller design and its implementation, respectively. The computation of the control current $\mathbf{i}_c$ is presented in conjunction with the state space adaptive controller in Chapter 3. Its implementation is considered in Section 4.5.2.

In the presented application both the current control loop and the position control loop operate at the same sampling frequency. If a large bandwidth is required for the position control loop, e.g. for a high speed rotor, it is advisable to implement the current control loop at a higher sampling frequency, or alternatively use an analogue circuit instead.

Although the controller uses floating point numbers, it has to convert all numbers to a fixed point representation for the analogue to digital conversion and vice versa. The quantisation, however, is symbolically ascribed to the ADCs and DACs.

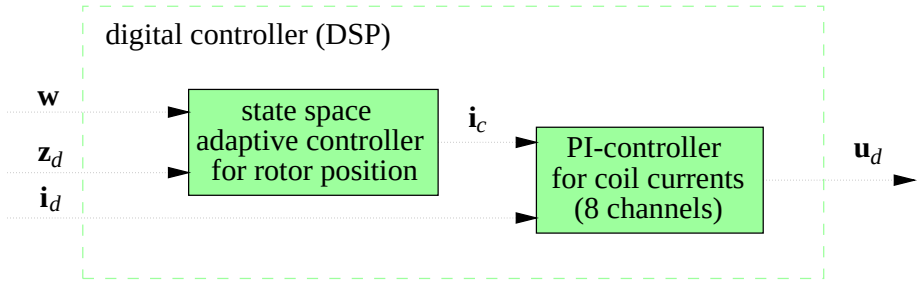

inputs: $\mathbf{w}$ set point
$\mathbf{z}_d$ sampled position
$\mathbf{i}_d$ sampled current

output: $\mathbf{u}_d$ digital control voltage

internal variable: $\mathbf{i}_c$ control current

Figure 2.3: Block diagram of the digital controller with its cascaded position and current controller.

2.2.2 Digital to analogue converter for control voltage

The task of the DACs (8 channels) is to convert the fixed point numbers provided by the DSP into an analogue voltage signal. Input is the digital control voltage $\mathbf{u}_d$, output the analogue control voltage $\boldsymbol{u}_a$ for all magnets of all bearing actuators. The DAC introduces quantisation noise and time delay which is modelled by a series of saturation, quantiser and time delay with the parameters given in Tab. 2.1. The corresponding SIMULINK block diagram is shown in Fig. D.3 in Appendix D.1.

Table 2.1: Parameters of DAC.

Bit resolution	12	-
Output voltage range	0-5	V
Quantisation	2.44	μm
Conversion delay	3	μs

2.2.3 Pulse width modulator (PWM) with switching amplifier and current sensor

Since the power losses of a linear amplifier would be too high, a switching amplifier is used in conjunction with a pulse width modulator (8 channels). Of course, this type of amplifier also introduces noise into the system at the harmonics of the switching frequency. Input to the PWM is the analogue control voltage $\boldsymbol{u}_a$ for all magnets of

both bearing actuators, output is the switched voltage $\boldsymbol{u}_s$. The PWM in conjunction with the switching amplifier is modelled as a saw-tooth generator modulating the input, a comparator, and two voltage sources with the parameters given in Tab. 2.2. Of course, a current saturation has to be included as a concession to reality. The corresponding SIMULINK block diagram is shown in Fig. D.6 in Appendix D.1.

Table 2.2: Parameters of PWM and switching amplifier

Input voltage range	0-5	V
Switching frequency	60	kHz
Switching voltage U_s	75	V
Maximal current	8	A
Amplifier gain K_a	30	-

From the modelling point of view, the coil current is output of the coil when a certain voltage is applied to it assuming the voltage source to be a pure effort source (voltage is independent of the drained current). Therefore, the current output $\boldsymbol{i}$ is logically assigned to the magnet model and is an input to the switching amplifier, because in a real application the current sensors are mounted on the switching amplifier boards. These sensors deliver the measured current signals $\boldsymbol{i}_m$.

2.2.4 Bearing actuator model

The rigid rotor is suspended in two active magnetic bearings. Inputs to these actuators are the switched voltages $\boldsymbol{u}_s = [\boldsymbol{u}_{s_A},\ \boldsymbol{u}_{s_B}]^T$ and the rotor position in bearing coordinates $\boldsymbol{z}_b = [\boldsymbol{z}_{b_A}, \boldsymbol{z}_{b_B}]^T$. Outputs are the actuator forces $\boldsymbol{F}_a = [\boldsymbol{F}_{a_A}, \boldsymbol{F}_{a_B}]^T$ and the currents in each coil $\boldsymbol{i} = [\boldsymbol{i}_A,\ \boldsymbol{i}_B]^T$. The parameters of both actuators are identical and given in Tab. 2.3.

For the sake of simplicity, only one bearing actuator as shown in Fig. 2.4 is presented. Omitting the suffix A for bearing A and B for bearing B the inputs to one bearing are the switched voltages $\boldsymbol{u}_s = [u_1, u_2, u_3, u_4]$ and the rotor position in bearing coordinates $\boldsymbol{z}_b = [x, y]$, the outputs are the actuator forces $\boldsymbol{F}_a = [F_x, F_y]$ with

$$F_x = F_1 - F_3 \tag{2.1}$$
$$F_y = F_2 - F_4, \tag{2.2}$$

and four currents $\boldsymbol{i} = [i_1, i_2, i_3, i_4]$ of the coils. The air gap lengths between rotor and magnet poles are determined by

$$l_1 = l_0 - x, \tag{2.3}$$
$$l_2 = l_0 - y, \tag{2.4}$$
$$l_3 = l_0 + x, \tag{2.5}$$
$$l_4 = l_0 + y. \tag{2.6}$$

The corresponding SIMULINK block diagram is shown in Fig. D.4 in Appendix D.1.

Table 2.3: Parameters of an active magnetic bearing

μ_0	permeability in vacuum	$4\,\pi \cdot 10^{-7}$	Vs/Am
μ_{r_s}	relative permeability of stator material	2000	-
μ_{r_r}	relative permeability of rotor material	1000	-
l_s	length of magnetic path in stator	$84 \cdot 10^{-3}$	m
l_r	length of magnetic path in rotor	$20 \cdot 10^{-3}$	m
A_s	cross section area of magnetic path in stator	$700 \cdot 10^{-6}$	m^2
A_r	cross section area of magnetic path in rotor	$420 \cdot 10^{-6}$	m^2
A_l	cross section area of magnetic path in air	A_s	m^2
B_{max_s}	maximum induction of stator material	1.3	T
B_{max_r}	maximum induction of rotor material	1.95	T
α	angle between pole shoes	$\pi/4$	rad
r	ohmic resistance in coil	0.8	Ω
N	number of coil windings = 2 pole shoes	130	-
l_0	nominal air gap	$0.5 \cdot 10^{-3}$	m
i_0	bias-current	4	A
L_0	nominal inductivity	0.01325	H
$\mathcal{R}_0$	nominal reluctance	$1.22 \cdot 10^6$	A/Vs

Nonlinear electromagnet model

Since all electromagnets of a bearing actuator are equal in design, only one is presented here without the suffices $j = 1, 2, 3, 4$ of their position. The input to a electromagnet is the voltage u and the air gap length l, output is the magnetic air-gap force F, which is always an attractive one. An additional output of each electromagnet is the coil current i. For one magnet the following equations for the voltage u, the magnetic flux Φ, the magnetic field strength H and the applied magneto-motive force $N\,i$ hold

$$N \frac{d\,\Phi}{d\,t} = u - r\,i, \tag{2.7}$$

$$N\,i = \oint H dl\,. \tag{2.8}$$

The magneto-motive force $N\,i$ can be rewritten in a discretised form

$$\oint H dl \approx \sum_i H_i\,l_i = H_r\,l_r + H_s\,l_s + 2\,H_l\,l. \tag{2.9}$$

With the constitutive law for the induction $B = \mu\,H$ and with $\Phi = A\,B$ for all cross sections the magnetic circuit is described by

$$N\,i = \mathcal{R}\,\Phi, \tag{2.10}$$

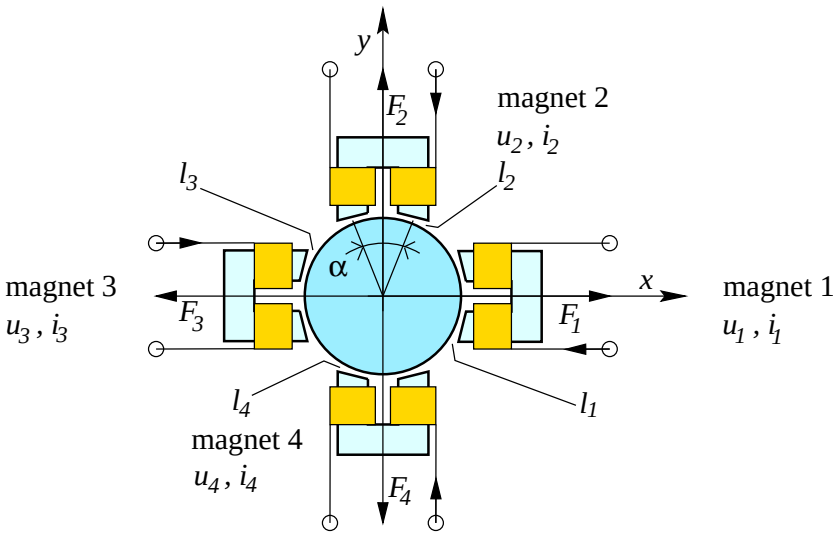

Figure 2.4: Sketch of an active magnetic bearing with four electro magnets, four voltage inputs u_j, four currents i_j and four ponderomotoric air-gap forces F_j, $j = 1, 2, 3, 4$.

where its magnetic reluctance $\mathcal{R}$ depends on the air gap length l as

$$\mathcal{R}(l) = \frac{1}{\mu_0}\left[\frac{l_r}{A_r\,\mu_{r_r}} + \frac{l_s}{A_s\,\mu_{r_s}} + \frac{2\,l}{A_l}\right]. \tag{2.11}$$

Using the preceding equations, the state equations for a coil can be established with the input variable u, the modulating air gap length l, the state variable Φ, and the output variables F and i

$$\frac{d\Phi}{dt} = -\frac{r_0\,\mathcal{R}(l)}{N^2}\,\Phi + \frac{1}{N}\,u, \tag{2.12}$$

$$F = \frac{\Phi^2}{\mu_0\,A_l}\cos\frac{\alpha}{2}, \tag{2.13}$$

$$i = \frac{\mathcal{R}(l)\,\Phi}{N}. \tag{2.14}$$

For simulation purposes special attention has to be paid to the saturation of the magnetic material. Assuming the relation $B = \mu(B)\,H$, the permeability of the magnetic material is defined by the anhysteretic curve [Haferl, 1991, Wurmsdobler, 1992] with

$$\mu(B) = \mu_0\left[\frac{1-\mu_r}{\pi}\arctan K\frac{(|B| - B_{max})}{B_{max}} + \frac{1+\mu_r}{2}\right], \tag{2.15}$$

with K being a constant determining the slope at the maximal induction B_{max}. In the presented work this constant has been chosen to be $K = 12.5$ in order to suit to a measured anhysteretic curve.

This approach guarantees $\mu \approx \mu_0 \mu_r$ for small inductions B and $\mu = \mu_0$ for high inductions B with a continuous transition. A sketch for this approach can be seen in Fig. 2.5. The anhysteretic function is implemented for both stator and rotor material.

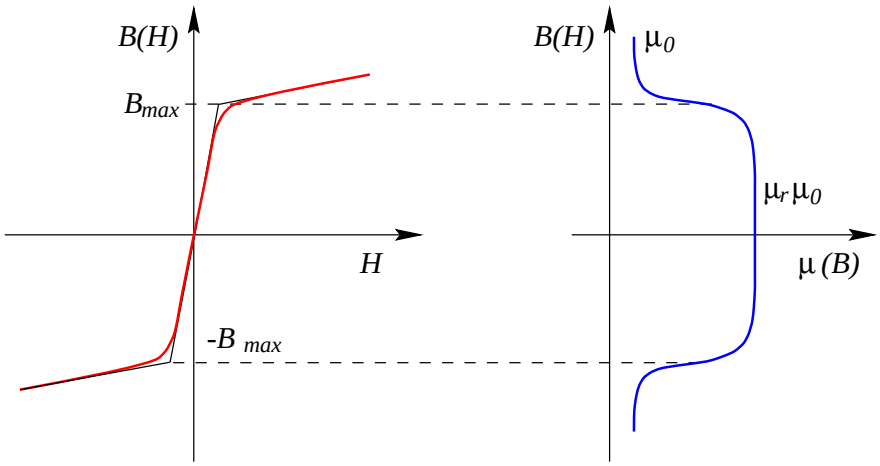

Figure 2.5: Anhysteretic curve with an induction dependent permeability $\mu(B)$.

As example, this function was computed for the stator material. The corresponding plot can be seen in Fig. 2.6

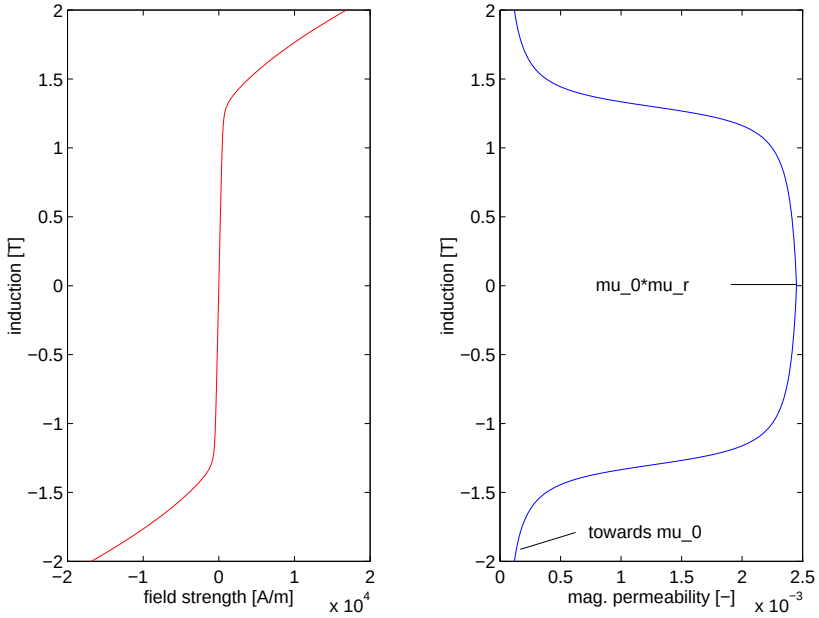

Figure 2.6: Anhysteretic curve with an induction dependent permeability $\mu(B)$ for the stator material.

Within the simulation two bearing actuators have to be implemented with four electromagnet models each. For this sake Eqn.(2.12), Eqn.(2.12) and Eqn.(2.12) have to be translated into a SIMULINK model using the definition for the magnetic reluctance $\mathcal{R}(l)$ in Eqn.(2.11). As mentioned previously, the relative permeability depends on the induction B within the simulation model. Therefore, Eqn.(2.15) has to implemented for each electromagnet for both the stator and the rotor material. The corresponding SIMULINK block diagram is shown in Fig. D.7 in Appendix D.1.

2.2.5 Rotor model

Figure 2.7 shows a sketch of the rotor bearing system under investigation. The rigid rotor is suspended by two active magnetic bearings at positions A' and B'. Two sensors are mounted perpendicularly to the shaft axis at the positions A" and B". Non-conservative self-exciting forces are expected to act in the plane N'. All system parameters used for numerical simulation are shown in Tab. 2.4.

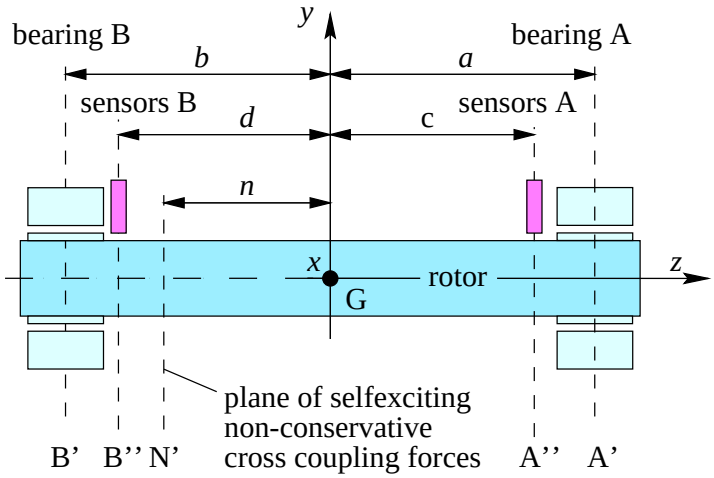

Figure 2.7: Sketch of a rigid rotor suspended by two magnetic bearings and excited by non-conservative cross-coupling forces at position N'. G denotes the centre of mass.

Inputs to the rotor are the actuator forces $\boldsymbol{F}_a$ at positions A' and B', outputs are the rotor positions $\boldsymbol{z}_s$ and $\boldsymbol{z}_b$ in the sensor planes and in bearing planes, respectively. The second order equation of motion for a rigid rotor with its degrees of freedom expressed by the bearing coordinates $\boldsymbol{z}_b = [x_A, y_A, x_B, y_B]^T$ is given by

$$\boldsymbol{M}_b\, \ddot{\boldsymbol{z}}_b + \boldsymbol{G}_b\, \dot{\boldsymbol{z}}_b + \boldsymbol{N}_b\, \boldsymbol{z}_b = \boldsymbol{F}_a + \boldsymbol{F}_w, \tag{2.16}$$

with the input bearing force vector $\boldsymbol{F}_a = [F_{x_A}, F_{y_A}, F_{x_B}, F_{y_B}]^T$ and the force vector corresponding to the rotor weight expressed by bearing coordinates

$$\boldsymbol{F}_w = -\frac{m_r\, g}{a-b} \begin{bmatrix} 0 & -b & 0 & a \end{bmatrix}^T. \tag{2.17}$$

Table 2.4: Parameters of rigid rotor suspended in two active magnetic bearings

g	earth acceleration	9.81	m/s^2
m_r	rotor mass	28.7680	kg
I_a	axial mass moment of inertia	0.8632	kgm^2
I_p	polar mass moment of inertia	0.02188	kgm^2
a	distance to bearing A	0.23877	m
b	distance to bearing B	-0.24123	m
c	distance to sensor A	0.18977	m
d	distance to sensor B	-0.19233	m
n	distance to plane N'	-0.1	m
k_n	non-conservative cross-coupling stiffness	0-10^7	N/m
Ω	rotor speed	$20,000$	rpm

All matrices are determined by a transformation from the coordinates of the centre of gravity $\boldsymbol{z}_c = [\phi_c, x_c, \psi_c, y_c]^T$ into bearing coordinates $\boldsymbol{z}_b$ using $\boldsymbol{z}_b = \boldsymbol{T}\,\boldsymbol{z}_c$ in the form

$$\boldsymbol{M}_b = \boldsymbol{T}^{-T}\,\boldsymbol{M}_c\,\boldsymbol{T}^{-1}, \tag{2.18}$$

$$\boldsymbol{G}_b = \boldsymbol{T}^{-T}\,\boldsymbol{G}_c\,\boldsymbol{T}^{-1}, \tag{2.19}$$

$$\boldsymbol{N}_b = \boldsymbol{T}^{-T}\,\boldsymbol{T}_n^T\,\boldsymbol{N}_n\,\boldsymbol{T}_n\,\boldsymbol{T}^{-1}, \tag{2.20}$$

with the mass matrix of the rotor

$$\boldsymbol{M}_c = \begin{bmatrix} I_a & 0 & 0 & 0 \\ 0 & m_r & 0 & 0 \\ 0 & 0 & I_a & 0 \\ 0 & 0 & 0 & m_r \end{bmatrix}, \tag{2.21}$$

and its gyroscopic matrix

$$\boldsymbol{G}_c = \begin{bmatrix} 0 & 0 & I_p & 0 \\ 0 & 0 & 0 & 0 \\ -I_p & 0 & 0 & 0 \\ 0 & 0 & 0 & 0 \end{bmatrix} \Omega, \tag{2.22}$$

corresponding to $\boldsymbol{z}_c$. The geometrical transformation matrices are given by

$$\boldsymbol{T} = \begin{bmatrix} a & 1 & 0 & 0 \\ 0 & 0 & a & 1 \\ b & 1 & 0 & 0 \\ 0 & 0 & b & 1 \end{bmatrix}, \tag{2.23}$$

$$\boldsymbol{T}_n = \begin{bmatrix} n & 1 & 0 & 0 \\ 0 & 0 & n & 1 \end{bmatrix}, \tag{2.24}$$

and the matrix of the self-exciting non-conservative cross-coupling coefficients in the plane N' has the form

$$\boldsymbol{N}_n = \begin{bmatrix} 0 & k_n \\ -k_n & 0 \end{bmatrix}. \tag{2.25}$$

The output vector $\boldsymbol{z}_s = [x_{s_A}, y_{s_A}, x_{s_B}, y_{s_B}]^T$ in sensor coordinates is determined by

$$\boldsymbol{z}_s = \boldsymbol{T}_s \, \boldsymbol{z}_c = \boldsymbol{T}_s \, \boldsymbol{T}^{-1} \, \boldsymbol{z}_b, \tag{2.26}$$

with

$$\boldsymbol{T}_s = \begin{bmatrix} c & 1 & 0 & 0 \\ 0 & 0 & c & 1 \\ d & 1 & 0 & 0 \\ 0 & 0 & d & 1 \end{bmatrix}. \tag{2.27}$$

For the use in a simulation, all these equations are modelled with SIMULINK built-in functions as it can be seen in the block diagram as shown in Fig. D.9 in Appendix D.1.

2.2.6 Position sensors

The position sensors have the input $\boldsymbol{z} = \boldsymbol{z}_s + \boldsymbol{v}$, where $\boldsymbol{v}$ is the measurement noise having a maximal deflection of v μm and a covariance matrix $\boldsymbol{Q} = \mathcal{E}\left\{ \boldsymbol{v}\boldsymbol{v}^T \right\}$. $\boldsymbol{z}_s$ is the rotor position vector at the sensor stations. The sensors provide the measured rotor displacements $\boldsymbol{z}_m = k_m \, \boldsymbol{z}$ with the parameters given in Tab. 2.5. It is assumed that the rotor rotation does not cause additional, periodic run-out errors.

Table 2.5: Parameters of position sensors

Sensor gain k_m	10^6	-
Measurement noise v	1	μm
Noise covariance $\mathbf{Q}$	$\mathbf{I}$	μm^2

Usually the measurement includes a conversion from rotor displacement in meters to V and within the DSP into m again. The measurement process is short cut by the conversion constant k_m for sake of simplicity. Additionally, the gain k_m is introduced to convert the position signals $\boldsymbol{z}$ from m to μm, because the simulation is carried out in m.

2.2.7 ADC for measured rotor positions

Input to the ADCs are the measured positions $\boldsymbol{z}_m$, output the sampled position values $\mathbf{z}_d$ (4 channels). Since the position in m is transformed into V, then converted into the discrete domain, and later on converted into μm, the conversion process is simulated by a series of quantiser, time delay and saturation with the parameters in Tab. 2.6. The corresponding SIMULINK block diagram is shown in Fig. D.8 in Appendix D.1.

Table 2.6: Parameters of ADC for position sensors

Input position range	± 250	μm
Bit resolution	10	-
Quantisation for position	0.489	μm
Conversion delay	3	μs

2.2.8 ADCs for measured currents

Current sensors (LEM-modules) are located on the switching amplifier boards and provide the measured coil currents $\boldsymbol{i}_m$ of all actuators. Inputs to the ADCs (8 channels) are the measured coil currents $\boldsymbol{i}_m$, outputs are the sampled current values $\mathbf{i}_d$ for all magnets of all actuators. Since the current (in A) is output in V, then converted into the discrete domain, and finally re-converted into A, the conversion process is simulated by a series of quantiser, time delay and saturation, with the parameters in Tab. 2.7, similarly to the ADCs for the position signals. The corresponding SIMULINK block diagram is shown in Fig. D.5 in Appendix D.1.

Table 2.7: Parameters of ADC for current sensors

Input current range	$0-8$	A
Bit resolution	9	-
Quantisation for current	0.0157	A
Conversion delay	3	μs

2.3 Model linearisation

The goal for the linearisation process is to derive a linear state space model of the nonlinear rotor bearing system as described above. Several steps are necessary to derive such a state space model.

1. A point of operation has to be defined for the rotor bearing system, i.e. for all energy storing state variables [Cellier, 1991]. From here, the entire system can be expected to behave linearly within a certain range of all state variables involved.

2. A current control loop is introduced. This loop guarantees the coil current to follow the control current from the point of operation within a certain bandwidth and reduces the order of the state space model.

3. Assuming the coil current as an independent input, a linear model for an electromagnet has to be derived for the point of operation.

4. A linear model for the magnetic actuator is derived. Below a certain frequency depending on the current controller the actuator can be treated as linear gain with respect to the control current and with respect to the rotor displacement.

5. A linear state space model of the rotor bearing system can be derived with control currents as input and rotor position as output.

An alternative solution is to control the rotor bearing system using a comprehensive state space controller including the states of all coils of both actuators. This approach, however, is not appropriate for adaptive control, because the number of parameters to be estimated becomes too large. Therefore, control is done by a cascaded current controller and a position controller. Note that the subsequently derived position controller always requires an underlying current control loop.

In the following subsections the presented steps lead to a linear actuator model and end up with a discrete time, linear state space model in controller canonical form.

2.3.1 Point of operation

The point of operation is defined by steady state values for all state variables involved in the rotor bearing system. In the present investigation these are the rotor position, the rotor velocity, and all fluxes of all electromagnets of both magnetic actuators defined by the bias current. This bias current is 4 A for the present application. The rotor position and velocity are zero for the point of operation.

2.3.2 Current control loop

The position control loop basically consists of the magnetic actuator, the current sensors, the ADCs, the controller, the DACS, the PWMs and the switching power amplifier. However, the conversion delay of 3 μs for the ADCs and DACs is negligible in comparison with the sample time of 100 μs. Therefore, not all subsystems have to be included for the linear model. Sensors, ADCs and DACs can be regarded as a unit gain with quantisation noise corrupting the output. The only subsystems remaining to be linearised are the electrical power signal path including the current measurement, the current controller, the switching power amplifier, and the electromagnets with the magnet force as output.

Linearisation of the current control loop

For two active magnetic bearings with four magnets each, in total 8 channels are necessary to be controlled. The controller for the current loop is implemented in the DSP as well, but logically separated from the position control loop.

The switching power amplifier with its PWM can be treated as gain with modulation noise depending on the input. The gain of the amplifier is determined by the ratio

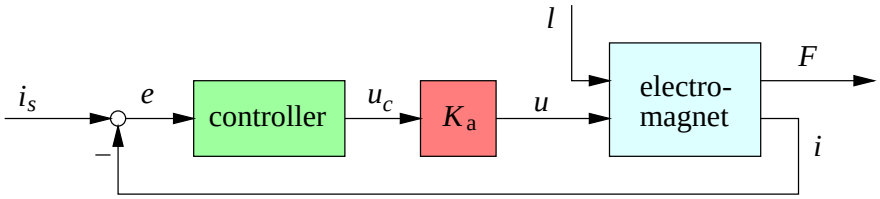

Figure 2.8: Block diagram of the current control loop with input i_s as the desired current, the air gap length l as the disturbance, the output F as the actuator force. K_a denotes the amplifier gain, e the control error, u_c the control voltage and u the input voltage to the electromagnet.

between switching voltage range and output voltage range of the DAC, in this case $150/5 = 30$.

Finally, the series DAC, PWM and switching amplifier is replaced by a gain $K_a = 30$, the series sensor and ADC by a unit gain. This means that the measured and sampled currents $\mathbf{i}_d$ are assumed to be the true currents $\boldsymbol{i}$. The corresponding block diagram can be seen in Fig. 2.8.

For a current controller design, a linear model for the electromagnet has to be derived from the nonlinear model presented in Section 2.2.4. How the digital control voltages $\mathbf{u}_d$ are computed from the control voltages $\mathbf{u}_c$, is described in Section 4.1.2.

Linearisation of an electromagnet

Given the point of operation defined by i_0 and l_0 for a centred rotor, the nonlinear Eqn.(2.12) to Eqn.(2.14) can be rewritten as

$$\frac{d\Phi}{dt} = \dot{\Phi}(\Phi(t), \mathcal{R}(l(t)), u(t)), \tag{2.28}$$

$$F = F(\Phi(t)), \tag{2.29}$$

$$i = i(\Phi(t), \mathcal{R}(l(t))) \tag{2.30}$$

and can be linearised with respect to the deviation variables $\Delta\Phi = \Phi - \Phi_0$, $\Delta F = F - F_0$, $\Delta i = i - i_0$ in the form

$$\frac{d(\Delta\Phi)}{dt} = -K_{\dot{\Phi}\Phi}\,\Delta\Phi + K_{\dot{\Phi}l}\,\Delta l + K_{\dot{\Phi}u}\,\Delta u \tag{2.31}$$

$$\Delta F = K_{F\Phi}\,\Delta\Phi \tag{2.32}$$

$$\Delta i = K_{i\Phi}\,\Delta\Phi + K_{il}\,\Delta l \tag{2.33}$$

using the partial derivatives

$$-K_{\dot{\Phi}\Phi} = \left.\frac{\partial\dot{\Phi}}{\partial\Phi}\right|_0 = -\frac{r\,\mathcal{R}_0}{N^2}, \tag{2.34}$$

$$K_{\dot{\Phi}l} = \left.\frac{\partial\dot{\Phi}}{\partial l}\right|_0 = \left.\frac{\partial\dot{\Phi}}{\partial\mathcal{R}}\cdot\frac{\partial\mathcal{R}}{\partial l}\right|_0 = -\frac{2\,r\,\Phi_0}{\mu_0\,N^2\,A_l}, \tag{2.35}$$

$$K_{\dot{\Phi}u} = \left.\frac{\partial\dot{\Phi}}{\partial u}\right|_0 = \frac{1}{N}, \tag{2.36}$$

$$K_{F\Phi} = \left.\frac{\partial F}{\partial\Phi}\right|_0 = \frac{2\,\Phi_0}{\mu_0\,A_l}\cos\frac{\alpha}{2}, \tag{2.37}$$

$$K_{i\Phi} = \left.\frac{\partial i}{\partial\Phi}\right|_0 = \frac{\mathcal{R}_0}{N}, \tag{2.38}$$

$$K_{il} = \left.\frac{\partial i}{\partial l}\right|_0 = \left.\frac{\partial i}{\partial\mathcal{R}}\cdot\frac{\partial\mathcal{R}}{\partial l}\right|_0 = \frac{2\,\Phi_0}{\mu_0\,N\,A_l}, \tag{2.39}$$

and the quantities for the point of operation

$$\mathcal{R}_0 = \frac{1}{\mu_0}\left[\frac{l_r}{A_r\,\mu_{r_r}} + \frac{l_s}{A_s\,\mu_{r_s}} + \frac{2\,l_0}{A_l}\right] \quad \text{and} \quad \Phi_0 = \frac{N\,i_0}{\mathcal{R}_0}. \tag{2.40}$$

Transforming Eqn.(2.31) to Eqn.(2.33) into the Laplace-domain and solving for $\Delta F(s)$ and $\Delta i(s)$ yields

$$\Delta F(s) = G_{lF}(s)\,\Delta l(s) + G_{uF}(s)\,\Delta u(s), \tag{2.41}$$

$$\Delta i(s) = G_{li}(s)\,\Delta l(s) + G_{ui}(s)\,\Delta u(s). \tag{2.42}$$

with the transfer functions

$$G_{lF}(s) = \frac{K_{F\Phi}\,K_{il}}{s + K_{\dot{\Phi}\Phi}}, \tag{2.43}$$

$$G_{uF}(s) = \frac{K_{F\Phi}\,K_{iu}}{s + K_{\dot{\Phi}\Phi}}, \tag{2.44}$$

$$G_{li}(s) = \frac{K_{i\Phi}\,K_{\dot{\Phi}l} + [s + K_{\dot{\Phi}\Phi}]\,K_{il}}{s + K_{\dot{\Phi}\Phi}}, \tag{2.45}$$

$$G_{ui}(s) = \frac{K_{i\Phi}\,K_{\dot{\Phi}u}}{s + K_{\dot{\Phi}\Phi}}. \tag{2.46}$$

For the sake of simplicity a continuous time PI-controller is introduced in the form

$$G_c(s) = \frac{\Delta u_c(s)}{\Delta e(s)} = K_c\,\frac{s + K_{\dot{\Phi}\Phi}}{s}. \tag{2.47}$$

Thus, all transfer functions for the linearised system are defined. The corresponding block diagram can be seen in Fig. 2.9.

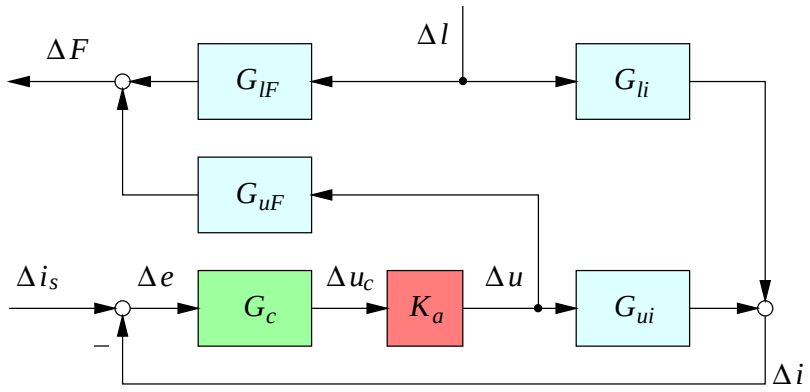

Figure 2.9: Block diagram of the linear current control loop with input Δi_s and Δl, and the output ΔF.

Current controller design

The current controller design is carried out in the continuous time domain, because the physical behaviour is more transparent than in the discrete time domain. In the present case, the zero of the proposed controller cancels the slow pole of the electromagnet. Thus, the plant transfer function results in

$$G_p(s) = G_c(s)\, K_a\, G_{ui}(s) = \frac{K_c\, K_a\, \mathcal{R}_0}{N^2\, s}. \tag{2.48}$$

This means that the phase lag is theoretically -90 deg over the entire frequency range and the controller gain can be chosen arbitrarily to achieve a current control loop with unlimited bandwidth. In reality, there are restrictions like saturation and a natural phase lag due to the sampling process and conversion delay. Approximating the zero-order sample hold element by a first order delay (Pade approximation)

$$H_0(s) = \frac{1}{1 + \frac{T_s}{2}\, s}, \tag{2.49}$$

the open loop transfer function is rewritten as

$$G_o(s) = \frac{K_c\, K_a\, \mathcal{R}_0}{N^2\, s\, (1 + \frac{T_s}{2}\, s)}. \tag{2.50}$$

The controller gain is determined for a certain phase margin and a maximum bandwidth using the frequency plots. Finally, the reference transfer function can be calculated as

$$G_{ii_s}(s) = \frac{\Delta i}{\Delta i_s} = \frac{\omega_n^2}{s^2 + 2\,\zeta\,\omega_n\, s + \omega_n^2}, \tag{2.51}$$

with the relations between the undamped eigenfrequency ω_n and the damping factor ζ

$$\omega_n^2 = \frac{2\, K_c\, K_a\, \mathcal{R}_0}{N^2\, T_s} \tag{2.52}$$

$$2\,\zeta\,\omega_n = \frac{2}{T_s}. \tag{2.53}$$

Note that the resulting reference transfer function is an approximation for the real system being controlled by a digital controller. Additionally, the zero order hold element is only used for control design purposes. An alternative solution is the z-transformation of the plant transfer function and the control design in the discrete time domain.

The numerical results for the controller design are presented in Section 4.1.1. The implementation is explained in detail in Subsection 4.1.2.

2.3.3 Linearised model of an electromagnet with underlying current control loop

Once the current control loop has been designed, the coil current can be assumed to be the desired one within a certain bandwidth. Therefore, the behaviour of the actuator consisting of four electromagnets must not depend on the controller properties. In the following the linearised model of an electromagnet with a current control loop is derived.

Conventional approach

In this model the output of the electromagnet is the ponderomotoric air-gap force following the law

$$F = \frac{\Phi(i,l)^2}{\mu_0 A_l} \cos\frac{\alpha}{2}, \tag{2.54}$$

with the magnetic flux

$$\Phi(i,l) = \frac{N\,i}{\mathcal{R}(l)}, \tag{2.55}$$

depending on the coil current $i = i_0 + \Delta i$ and the magnetic reluctance $\mathcal{R}(l)$ which is a function of the air-gap length $l = l_0 + \Delta l$. For the point of operation defined by i_0 and l_0, the linear relation for the magnet force is

$$\Delta F = K_{lF}\,\Delta l + K_{iF}\,\Delta i, \tag{2.56}$$

with the partial derivatives

$$K_{iF} = \left.\frac{\partial F}{\partial i}\right|_0 = \frac{2\,N^2\,i_0}{\mathcal{R}_0^2\,\mu_0\,A_l}\cos\frac{\alpha}{2}, \tag{2.57}$$

$$K_{lF} = \left.\frac{\partial F}{\partial l}\right|_0 = \left.\frac{\partial F}{\partial \mathcal{R}}\cdot\frac{\partial \mathcal{R}}{\partial l}\right|_0 = -\frac{4\,N^2\,i_0^2}{\mathcal{R}_0^3\,\mu_0^2\,A_l^2}\cos\frac{\alpha}{2}, \tag{2.58}$$

being the steady state coefficients for an electromagnet with respect to the air-gap forces.

Non conventional approach

From the control point of view, the coil current cannot be assumed to be identical with the desired current, i.e. the electromagnet cannot be treated independently from the controller. This can only be the case for low frequencies, where the reference transfer function G_w behaves like a gain, or at least for a steady state. Therefore, an alternative derivation of the characteristic steady state coefficients K_{lF} and K_{iF} for an electromagnet is presented in the following.

Using the expressions $\Delta u(s) = K_a\,\Delta u_c(s)$ and $\Delta e(s) = \Delta i_s(s) - G_{ii_s}(s)\,\Delta i_s(s)$ the voltage for one electromagnet becomes

$$\Delta u(s) = \frac{G_c(s)\,K_a}{1 + G_c(s)\,K_a\,G_{ui}(s)}\,\Delta i_s(s) - \frac{G_{li}(s)\,G_c(s)\,K_a}{1 + G_c(s)\,K_a\,G_{ui}(s)}\,\Delta l(s). \tag{2.59}$$

Finally, using this result and the above definition for $\Delta F(s)$, the magnet force can be written as a linear combination such that

$$\Delta F(s) = G_{lFc}(s)\,\Delta l(s) + G_{iFc}(s)\,\Delta i_s(s), \tag{2.60}$$

with the transfer functions

$$G_{iFc}(s) = \frac{G_{uF}(s)\,G_c(s)\,K_a}{1 + G_c(s)\,K_a\,G_{ui}(s)}, \tag{2.61}$$

$$G_{lFc}(s) = \frac{G_{lF}(s)\;[1 + G_c(s)\,K_a\,G_{ui}(s)] - G_{uF}(s)\,G_{li}(s)\,G_c(s)\,K_a}{1 + G_c(s)\,K_a\,G_{ui}(s)}. \tag{2.62}$$

Inserting the above defined transfer functions and the partial derivatives at the point of operation, these functions result in

$$G_{iFc}(s) = \frac{2\,K_a\,K_c\,\Phi_0\,N}{A_l\,\mu_0\;[K_a\,K_c\,\mathcal{R}_0 + N^2\,s]}\cos\frac{\alpha}{2}, \tag{2.63}$$

$$G_{lFc}(s) = -\frac{4\,\Phi_0^2\left[K_a\,K_c\,r\,\mathcal{R}_0 + N^2\;[K_a\,K_c\;+ r]\;s\right]}{A_l\,\mu_0^2\;[K_a\,K_c\,\mathcal{R}_0 + N^2\,s]\;[r\,\mathcal{R}_0 + N^2\,s]}\cos\frac{\alpha}{2}. \tag{2.64}$$

Utilising the definitions for $\mathcal{R}_0$ and Φ_0, the constant steady state coefficients for one electromagnet can be obtained from $s \to 0$ by

$$K_{iF} = G_{iFc}(s)\Big|_{s=0} = \frac{2\,N^2\,i_0}{\mathcal{R}_0^2\,\mu_0\,A_l}\cos\frac{\alpha}{2}, \tag{2.65}$$

$$K_{lF} = G_{lFc}(s)\Big|_{s=0} = -\frac{4\,N^2\,i_0^2}{\mathcal{R}_0^3\,\mu_0^2\,A_l^2}\cos\frac{\alpha}{2}. \tag{2.66}$$

It does not surprise that the coefficients are independent of the controller parameters as long as there is no steady state error between the desired current and the actual coil current. This is only the case if a PI-controller is used for the current control task.

Note that a continuous time controller was used in the derivation above. This procedure has actually no influence on the steady state behaviour. The dynamical behaviour, however, is affected by a digital implementation. If the dynamics of the digital implementation is to be included, all transfer functions have to be transformed into the z-plane in order to obtain an accurate result.

2.3.4 Linearised actuator model

In this investigation an actuator consists of four electromagnets as shown in Fig. 2.4. Outputs are the actuator forces $\boldsymbol{F}_a = [F_x, F_y]$ and four currents $\boldsymbol{i} = [i_1, i_2, i_3, i_4]$ of all coils. A current control loop is implemented for all electromagnets with the desired currents

$$i_{s_1} = i_0 + i_x, \quad (2.67) \qquad i_{s_3} = i_0 - i_x, \quad (2.69)$$

$$i_{s_2} = i_0 + i_y, \quad (2.68) \qquad i_{s_4} = i_0 - i_y, \quad (2.70)$$

depending on the control currents $\boldsymbol{i}_c = [i_x, i_y]$ in x and y directions respectively, and the bias current i_0. From this point on, the dynamics of the current control loop is neglected, because the coil currents are expected to be equal to the desired ones ($i_{s_j} \stackrel{!}{=} i_j$ for $j = 1, 2, 3, 4$). This, however, requires an underlying current controller as a sub-task implemented in the DSP for all current loops.

Note that one has to distinguish between the desired currents i_{s_j} for $j = 1, 2, 3, 4$ which are absolute currents like the currents i_j, and the control current vector $\boldsymbol{i}_c$, which is the control variable of the position control loop assuming a linear actuator at the point of operation.

A linear model of an actuator can be derived using the assumptions for the air gap lengths defined by Eqn.(2.3) to Eqn.(2.6) in each electromagnet

$$F_x = F_1 - F_3 = K_s\, x + K_i\, i_x, \quad (2.71)$$

$$F_y = F_2 - F_4 = K_s\, y + K_i\, i_y, \quad (2.72)$$

with the current gain factor

$$K_i = 2\, K_{iF} = \frac{4\, N^2\, i_0}{\mathcal{R}_0^2\, \mu_0\, A_l} \cos\frac{\alpha}{2} \quad (2.73)$$

and the position stiffness

$$K_s = 2\, K_{lF} = -\frac{8\, N^2\, i_0^2}{\mathcal{R}_0^3\, \mu_0^2\, A_l^2} \cos\frac{\alpha}{2} \quad (2.74)$$

For the linear model, both bearing actuators are treated as one system with the control currents $\boldsymbol{i}_c = [\boldsymbol{i}_{c_A} \boldsymbol{i}_{c_B}]$ as input to the bearing, and the resulting actuator forces $\boldsymbol{F}_a = [\boldsymbol{F}_{a_A}, \boldsymbol{F}_{a_B}]^T$ as output. The linearised model of the active magnetic bearings is then given by the linear relation

$$\boldsymbol{F}_a = \boldsymbol{K}_s\, \boldsymbol{z}_b + \boldsymbol{K}_i\, \boldsymbol{i}_c \quad (2.75)$$

with the stiffness matrix in bearing coordinates $\boldsymbol{z}_b$ according to Fig. 2.10 $\boldsymbol{K}_s = K_s\, \mathbf{I}$, and the current gain matrix $\boldsymbol{K}_i = K_i\, \mathbf{I}$ with $\mathbf{I}$ being the 4×4 identity matrix.

2.3.5 Linear rotor bearing model

After the linear model for an electro-magnetic actuator has been derived in the previous section, only the mechanical part remains with the rigid rotor and the active magnetic bearing as a gain with respect to the control current input and a negative stiffness coefficient with respect to the rotor position.

Sensors and ADCs can be regarded as a unit gain with quantisation noise corrupting the output. All noise of any kind generated by the system is gathered within a system noise vector for the discrete time, linear, and stochastic state space model. No specific model is provided for the disturbances. The quantisation noise is gathered within an input noise vector.

Thus, the position control loop consists basically of the magnetic actuator, the rotor, the sensors, the ADCs and the controller. The conversion delay of $3\,\mu$s for the ADCs is negligible in comparison with the sample time of $100\,\mu$s. The conversion gain from m to μm is ascribed to the rotor model, which is linear itself. Starting with the linear continuous time model a stochastic discrete time state space model is derived in this section.

Linear continuous time model for the rotor magnetic bearing system

The rotor model itself is already linear, and the rotor weight $\boldsymbol{F}_w$ can be compensated by an additional constant control current

$$\boldsymbol{i}_{c_w} = \boldsymbol{K}_i^{-1} \cdot \boldsymbol{F}_w. \tag{2.76}$$

Using the linear actuator model derived above, the rotor bearing equations of motion can be described by

$$\boldsymbol{M}_b\,\ddot{\boldsymbol{z}}_b + \boldsymbol{G}\,\dot{\boldsymbol{z}}_b + (\boldsymbol{N}_b + \boldsymbol{K}_s)\,\boldsymbol{z}_b = \boldsymbol{K}_i\,\boldsymbol{i}_c, \tag{2.77}$$

with the input vector $\boldsymbol{i}_c = [i_{x_A}, i_{x_B}, i_{y_A}, i_{y_B}]^T$, consisting of the control currents of four active magnetic bearing axes. Actually, the control currents $\boldsymbol{i}_c$ only exist in the discrete domain as $\mathbf{i}_c$, but are assumed to be continuous for the derivation of the discrete state space model. The same is true for the set point vector $\mathbf{w}$. Figure 2.10 shows the linearised plant model.

Neglecting the transfer characteristics of the sensors, ADCs and DACs, the resulting continuous time state space model is then given in bearing coordinates in the form

$$\dot{\boldsymbol{x}}_b = \boldsymbol{A} \cdot \boldsymbol{x}_b + \boldsymbol{B} \cdot \boldsymbol{u}, \tag{2.78}$$

$$\boldsymbol{y} = \boldsymbol{C} \cdot \boldsymbol{x}_b + \boldsymbol{v}, \tag{2.79}$$

with the continuous time state vector $\boldsymbol{x}_b = [\boldsymbol{z}_b, \dot{\boldsymbol{z}}_b]^T$ (number of states $n_s = 8$), the output vector $\boldsymbol{y} = k_m(\boldsymbol{z}_b + \boldsymbol{v})$ (number of outputs $n_o = 4$), and the input vector $\boldsymbol{u} = \boldsymbol{i}_c$ (number of inputs $n_i = 4$). For numerical reasons a virtual sensor gain k_m converts the system states into μm. Using the output in μm yields parameters with reasonable ranges of value for both system matrices and controller parameters.

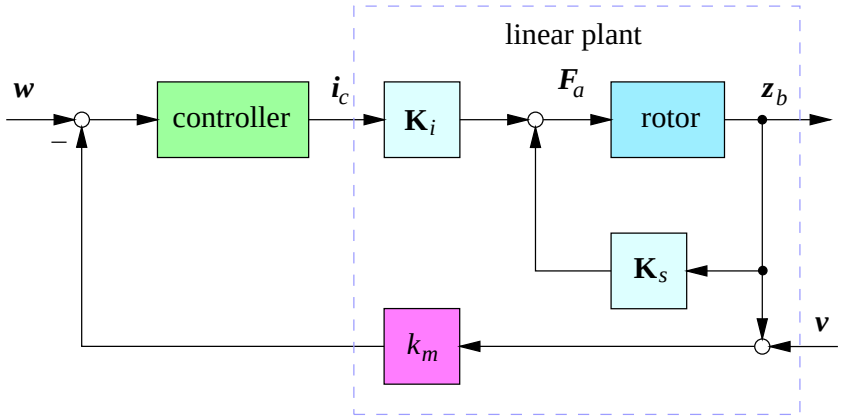

input: w set point
v measurement noise

output: z_b rotor position

internal variables:
i_c digital control voltage
F_a actuator forces

Figure 2.10: Block diagram of the linearised deterministic plant model.

Although the position is measured in the sensor planes, the proximity sensors are assumed to be collocated with the bearings for the linear model. This is justified for a rigid rotor model, because the displacements in the bearing planes $\boldsymbol{z}_b$ can easily be calculated from the sampled sensor signal $\boldsymbol{z}_d$ by the simple transformation (see Eqn.(2.26))

$$\boldsymbol{z}_b = \boldsymbol{T}\,\boldsymbol{T}_s^{-1}\,\boldsymbol{z}_d. \tag{2.80}$$

Similarly to $\mathbf{i}_d$, $\mathbf{z}_d$ already is a discrete vector, but is assumed to have the continuous equivalent $\boldsymbol{z}_d$.

The system matrices are defined as follows:

$$\boldsymbol{A} = \begin{bmatrix} \mathbf{0} & \mathbf{I} \\ -\boldsymbol{M}_b^{-1}\,(\boldsymbol{N}_b + \boldsymbol{K}_s) & -\boldsymbol{M}_b^{-1}\,\boldsymbol{G}_b \end{bmatrix}, \tag{2.81}$$

$$\boldsymbol{B} = \begin{bmatrix} \mathbf{0} \\ \boldsymbol{M}_b^{-1}\,\boldsymbol{K}_i \end{bmatrix}, \tag{2.82}$$

$$\boldsymbol{C} = \begin{bmatrix} k_m\,\mathbf{I} & \mathbf{0} \end{bmatrix}. \tag{2.83}$$

Deterministic discrete time state space model for the rotor bearing system

A transformation into a discrete time system with sampling time T_s yields the deterministic discrete state space model

$$\mathbf{x}_b(k+1) = \mathbf{\Phi}\,\mathbf{x}_b(k) + \mathbf{\Gamma}\,\mathbf{u}(k), \tag{2.84}$$
$$\mathbf{y}(k) = \boldsymbol{C}\,\mathbf{x}_b(k), \tag{2.85}$$

with its system matrices of no particular structure, namely the transition matrix and the discrete time control matrix (see [Föllinger, 1990])

$$\mathbf{\Phi} = e^{\boldsymbol{A}\cdot T_s} \quad \text{and} \tag{2.86}$$
$$\mathbf{\Gamma} = \left[e^{\boldsymbol{A}\cdot T_s} - \mathbf{I}\right] \cdot \boldsymbol{A}^{-1} \cdot \boldsymbol{B}. \tag{2.87}$$

Since the discrete state space model should have a minimum number of parameters to be identified, it is transformed into a canonical form. With respect to the calculation of an adaptive controller, a controller canonical form is chosen [Tolle, 1985]. For the reason of symmetry the structural indices are $\nu_i = 2$, which means that there are four coupled second order systems [Schumann, 1982, Tolle, 1985]. With the transformation

$$\mathbf{x} = \mathbf{T}\,\mathbf{x}_b \quad \text{and} \quad \mathbf{x}_b = \mathbf{T}^{-1}\,\mathbf{x} \tag{2.88}$$

using the transformation matrix $\mathbf{T}$ the new matrices are

$$\mathbf{A} = \mathbf{T}\,\mathbf{\Phi}\,\mathbf{T}^{-1}, \tag{2.89}$$
$$\mathbf{B} = \mathbf{T}\,\mathbf{\Gamma}, \tag{2.90}$$
$$\mathbf{C} = \boldsymbol{C}\,\mathbf{T}^{-1}. \tag{2.91}$$

Appendix A gives the derivation of the transformation $\mathbf{T}$. The entire deterministic model in canonical form can then be written as

$$\mathbf{x}(k+1) = \mathbf{A}\,\mathbf{x}(k) + \mathbf{B}\,\mathbf{u}(k), \tag{2.92}$$
$$\mathbf{y}(k) = \mathbf{C}\,\mathbf{x}(k), \tag{2.93}$$

with the (8×1)-state vector $\mathbf{x}(k)$. The (4×1)-input vector $\mathbf{u}(k)$ is the sampled input vector $\boldsymbol{u}(t)$ and the (4×1)-output vector $\mathbf{y}(k)$ is the sampled vector $\boldsymbol{y}(t)$. The (8×8)-system matrix $\mathbf{A} = \{\mathbf{A}^{(ij)}\}$ is partitioned into sub-matrices of the form

$$\mathbf{A}^{(ij)} = \begin{bmatrix} 0 & 1 \\ -a_2^{(ij)} & -a_1^{(ij)} \end{bmatrix}, \tag{2.94}$$

$$\mathbf{A}^{(ii)} = \begin{bmatrix} 0 & 0 \\ -a_2^{(ii)} & -a_1^{(ii)} \end{bmatrix}, \tag{2.95}$$

with $i, j = 1, 2, 3, 4$. The (8×4)-control matrix $\mathbf{B} = \{\boldsymbol{b}^{(ij)}\}$ is composed of

$$\boldsymbol{b}^{(ij)} = \begin{bmatrix} 0 & 1 \end{bmatrix}^T, \tag{2.96}$$
$$\boldsymbol{b}^{(ii)} = \begin{bmatrix} 0 & 0 \end{bmatrix}^T, \tag{2.97}$$

and the(4×8) measurement matrix $\mathbf{C} = \{\boldsymbol{c}^{T(ij)}\}$ is

$$\boldsymbol{c}^{T(ij)} = \left[\begin{array}{cc} c_2^{(ij)} & c_1^{(ij)} \end{array} \right]. \tag{2.98}$$

The matrices are computed numerically using the transformation matrix derived in Appendix A from the transition matrix and the discrete time control matrix according to Eqn.(2.86) and Eqn.(2.87), respectively.

Stochastic state space model for the rotor bearing system

Based upon the deterministic state space model defined in Eqn.(2.92) and Eqn.(2.93), the general stochastic state space model that is widely used in systems theory is

$$\begin{aligned} \mathbf{x}(k+1) &= \mathbf{A}\,\mathbf{x}(k) + \mathbf{B}\,\mathbf{u}(k) + \boldsymbol{\xi}(k), & (2.99)\\ \mathbf{y}(k) &= \mathbf{C}\,\mathbf{x}(k) + \boldsymbol{\eta}(k), & (2.100) \end{aligned}$$

with the sequences of independent random noise vectors as the (8×1)-system noise $\boldsymbol{\xi}(k)$ and the (4×1)-measurement noise $\boldsymbol{\eta}(k)$ with each vector being of zero mean

$$\begin{aligned} \mathcal{E}\,\{\,\boldsymbol{\xi}(k)\,\} &= \mathbf{0}, & (2.101)\\ \mathcal{E}\,\{\,\boldsymbol{\eta}(k)\,\} &= \mathbf{0}, & (2.102) \end{aligned}$$

and with the covariance matrices

$$\begin{aligned} \mathcal{E}\left\{\,\boldsymbol{\xi}(k)\boldsymbol{\xi}^T(k)\,\right\} &= \mathbf{R}_1, & (2.103)\\ \mathcal{E}\left\{\,\boldsymbol{\eta}(k)\boldsymbol{\eta}^T(k)\,\right\} &= \mathbf{R}_2, & (2.104)\\ \mathcal{E}\left\{\,\boldsymbol{\eta}(k)\boldsymbol{\xi}^T(k)\,\right\} &= \mathbf{R}_{12}. & (2.105) \end{aligned}$$

Within the system noise $\boldsymbol{\xi}(k)$ all noise generated within the system is modelled without an additional input matrix. The estimation of such an input matrix would not be possible, because the disturbances cannot be measured. All noise as generated by the ADCs and the measurement noise is gathered within the measurement noise vector $\boldsymbol{\eta}(k)$. The covariance matrices $\mathbf{R}_1$, $\mathbf{R}_2$ and $\mathbf{R}_{12}$ are generally not known, but can be estimated online.

This model structure yields 64 parameters to be estimated, although the matrices $\mathbf{A}$ with $n_s^2 = 64$ entries, $\mathbf{B}$ and $\mathbf{C}$ with $n_s\,n_i = 32$ and $n_s\,n_o = 32$ entries, respectively, have a total of 128 entries. This is due to the controller canonical form. Using this form, in the present case, only every second row of $\mathbf{A}$ contains parameters to be estimated, i.e. only $\frac{n_s^2}{2} = 32$ parameters. The control matrix $\mathbf{B}$ is fixed in its structure and can be omitted regarding parameter estimation, because it only contains zeros and ones. The measurement matrix has no particular structure which means that all 32 entries are parameters to be estimated.

Note, that these parameters are no longer parameters having a physical meaning, but are the result of various transformations. Additionally, the state vector $\mathbf{x}$ is not identical with the sampled state vector $\boldsymbol{x}_b$ of the original continuous time model.